SLAC-PUB-6327
November 1993
(T/E)

SLAC MEASUREMENTS OF THE NEUTRON SPIN-STRUCTURE FUNCTION*

GERASSIMOS G. PETRATOS
representing the SLAC E142 Collaboration

Stanford Linear Accelerator Center
Stanford University, Stanford, California 94309

ABSTRACT

Results from a measurement of the neutron spin-dependent structure function $g_1^n(x)$ over a range in x from 0.03 to 0.6 and with $Q^2 > 1$ (GeV/c)^2 are presented. The experiment consisted of scattering a longitudinally polarized electron beam from the Stanford Linear Accelerator off a polarized ^{3}He target and detecting scattered electrons in two magnetic spectrometers. The results are interpreted in the quark-parton model and used to test the Bjorken sum rule.

Presented at Hadron 93: Biennial Conference on Hadron Spectroscopy
Como, Italy, June 21-25, 1993.

* Work supported by Department of Energy contract DE-AC03-76SF00515.

The results of a measurement of the neutron spin structure function g_1^n in the Bjorken x range from 0.03 to 0.6 are presented. The experiment used a longitudinally polarized beam from the Stanford Linear Accelerator and a polarized ^{3}He target. The new measurement is complimentary to previous measurements of the proton spin structure function g_1^p at SLAC[1,2] and CERN.[3] Interpretation of the latter measurements in the context of the quark-parton model of the nucleon suggested that the quarks carry a small fraction of the proton spin and that the strange sea polarization is large and negative, a rather surprizing result.

The spin structure functions G_1 and G_2 of the nucleons are determined by measuring the cross section asymmetries[4,5]

$$A_{\parallel} = \frac{\sigma(\uparrow\Uparrow) - \sigma(\uparrow\Downarrow)}{\sigma(\uparrow\Uparrow) + \sigma(\uparrow\Downarrow)} = \frac{1-\epsilon}{(1+\epsilon R)W_1}\left[(E+E'\cos\theta)MG_1 - Q^2G_2\right], \qquad (1)$$

and

$$A_{\perp} = \frac{\sigma(\uparrow\Rightarrow) - \sigma(\uparrow\Leftarrow)}{\sigma(\uparrow\Rightarrow) + \sigma(\uparrow\Leftarrow)} = \frac{(1-\epsilon)E'}{(1+\epsilon R)W_1}\left[(MG_1 + 2EG_2)\sin\theta\right] \qquad (2)$$

in deep inelastic scattering of polarized electrons from polarized nucleons. Here $\uparrow$ and $\downarrow$ denote the longitudinal spin of the incoming electron (along or opposite the direction of its momentum), and $\Uparrow$ and $\Downarrow$ or $\Leftarrow$ and $\Rightarrow$ denote the longitudinal or transverse spin of the target nucleon. The asymmetries are functions of the nucleon mass M, the incident electron energy E, the scattered electron energy E' and angle θ, the degree of the longitudinal polarization of the virtual photon exchanged in the scattering $\epsilon = [1 + 2(1+\nu^2/Q^2)\tan^2(\theta/2)]^{-1}$, and the spin-averaged structure functions W_1 and W_2 which are related via $R = [(1+\nu^2/Q^2)W_2/W_1 - 1]$.

In the Bjorken scaling limit of large four-momentum $Q^2 = 4EE'\sin^2(\theta/2)$ and energy $\nu = E - E'$ transfers, the spin structure functions are predicted to become functions only of the Bjorken scaling variable $x = Q^2/2M\nu$, which is the fraction of the nucleon momentum carried by the struck quark in the scattering

$$M\nu^2 G_1(x, Q^2) \to g_1(x). \qquad (3)$$

$$M\nu^2 G_2(x,Q^2) \rightarrow g_2(x). \tag{4}$$

In the quark-parton model, the nucleon spin structure function $g_1(x)$ is related to the quark plus anti-quark momentum distributions $q_i(x)$:

$$g_1(x) = \sum_i z_i^2 [q_i^{\uparrow}(x) - q_i^{\downarrow}(x)], \tag{5}$$

where $\uparrow$ ($\downarrow$) represents spins parallel (anti-parallel) to the nucleon spin, and the sum is over all quark flavors of charge z_i. This structure function is also related to the asymmetry A_1 defined by (neglecting $g_2(x)$)

$$A_1(x) \cong \frac{A_{\parallel}}{D} \cong \frac{g_1(x)}{MW_1(x)}, \tag{6}$$

where $D = (1-\epsilon E'/E)/(1+\epsilon R)$ is the fraction of the incident electron polarization carried by the virtual photon. The A_1 asymmetry is a measure of the probability that the quark spins are aligned with the nucleon spin.

The spin structure functions g_1^p and g_1^n of the proton and neutron are related by the Bjorken sum rule[6] including first-order perturbative quantum chromodynamics (QCD) corrections[7]

$$\int_0^1 [g_1^p(x) - g_1^n(x)]dx = \frac{1}{6}\left|\frac{g_A}{g_V}\right|\left[1 - \frac{\alpha_s(Q^2)}{\pi}\right]. \tag{7}$$

where g_A and g_V are the weak couplings from nucleon beta decay, and $\alpha_s(Q^2)$ is the QCD coupling constant. This sum rule, first derived from current algebra and based on isospin symmetry, is a rigorous prediction of perturbative QCD.

Separate sum rules for the proton and neutron were derived by Ellis and Jaffe[8] assuming SU(3) symmetry and an unpolarized strange sea:

$$\int_0^1 g_1^p(x)dx \simeq \frac{1}{18}(9F - D)\left[\frac{1-\alpha_s(Q^2)}{\pi}\right], \quad \text{and} \tag{8}$$

$$\int_0^1 g_1^n(x)dx \simeq \frac{1}{18}(6F - 4D)\left[\frac{1-\alpha_s(Q^2)}{\pi}\right], \tag{9}$$

where F and D are SU(3) invariant matrix elements of the axial vector current.

The integrals over the spin structure functions have a simple interpretation in the quark-parton model:

$$\int_0^1 g_1^p(x)dx \simeq \frac{1}{2}(\frac{4}{9}\Delta u + \frac{1}{9}\Delta d + \frac{1}{9}\Delta s)\left[\frac{1-\alpha_s(Q^2)}{\pi}\right] \quad \text{and} \tag{10}$$

$$\int_0^1 g_1^n(x)dx \simeq \frac{1}{2}(\frac{1}{9}\Delta u + \frac{4}{9}\Delta d + \frac{1}{9}\Delta s)\left[\frac{1-\alpha_s(Q^2)}{\pi}\right]. \tag{11}$$

where the $\Delta q_i^{\uparrow} = \int_0^1 [q_i^{\uparrow}(x) - q_i^{\downarrow}(x)]dx$ represent the integrals over the momentum distributions of the up, down, and strange quarks of the nucleon. A measurement of the integrals of the spin structure functions in conjunction with the neutron beta decay relationship $\Delta u - \Delta d = F + D$ and the hyperon decay relationship $\Delta d - \Delta s = F - D$ can be used to solve for the $\Delta u, \Delta d$, and Δs quark spin distributions.

Polarized electrons with energies of 19 to 26 GeV and 2 μA intensity were produced by a laser optically pumped AlGaAs source (see Fig. 1). The helicity of the beam was reversed randomly on a pulse-to-pulse basis by reversing the circular polarization of the excitation photons. The beam polarization was

monitored during the experiment by measuring the cross section asymmetry in Moller scattering off polarized electrons in a magnetized ferromagnetic foil (see Fig. 2). Electrons scattered at 90° in the center-of-mass frame were detected in a magnetic spectrometer consisting of a dipole magnet and an array of proportional tubes. The beam polarization was found to be stable over the duration of the experiment with an average value of $(39 \pm 2)\%$ (see Fig. 3).

The experiment used a polarized ^{3}He target. The nucleon spin structure of a polarized ^{3}He target is the same as a polarized free neutron target to the extent that the ^{3}He nucleus is in a space-symmetric S state. In an S state, the two proton spins are aligned antiparallel due to the Pauli exclusion principle, implying that scattering from a polarized ^{3}He nucleus represents scattering from a polarized neutron. The presence of some S' and D state admixtures in the ^{3}He ground state complicates the above picture by introducing a polarized proton component opposite to that of the neutron. Theoretical calculations[9–11] have shown that these admixtures have a small effect in the cross section asymmetry measurements and that the theoretical uncertainty in extracting the spin structure function $g_1^n(x)$ is small (see Fig. 4).

The target is based on the technique of ^{3}He polarization by spin exchange collisions with Rb vapor.[12] The Rb atoms are polarized via laser optical pumping by absorbing circularly polarized photons at a wavelength of 795 nm. The spin exchange from Rb to ^{3}He occurs due to the hyperfine interaction between the polarized valence electron of Rb and the ^{3}He nucleus.

The major elements of the target system[14] are shown in Fig. 5. To avoid Rb depolarization by the beam, the optical pumping region is separated from the bombardment region by using a dual chamber target. The bottom chamber is a 30 cm glass tube with 0.012-cm-thick end windows, containing a ^{3}He density of 2.3×10^{20} cm^{-3} (9 atm at 0°C). The top chamber contains several milligrams of Rb metal, and is heated to ~180°C to obtain the desired density of Rb vapor. The lasers for optical pumping are five solid state titanium-sapphire lasers, each

pumped by an argon-ion laser and producing greater than 20 watts of power. The axis of quantization for polarization is established by the magnetic field produced by the two main Helmholtz coil sets. The drive and pickup coils are used for the ^{3}He polarization measurements.

The ^{3}He nuclear polarization was measured by means of nuclear magnetic resonance (NMR) adiabatic fast passage.[12] The ^{3}He NMR signals (see Fig. 6) were calibrated to the NMR signals of the proton polarization at thermal equilibrium in water (see Fig. 6). The water sample was contained in a cell identical to the ^{3}He bombardment cell. The average ^{3}He polarization was $\sim 35\%$, as can be seen in Fig. 7. The fractional uncertainty in the ^{3}He polarization measurement was $\pm 7\%$, dominated by uncertainties in the water calibration.

The neutron asymmetries were extracted from the ^{3}He measured asymmetries assuming[9] that the polarization of the neutron in ^{3}He is $\sim 87\%$. A correction for the polarization of the two protons in ^{3}He ($\sim -2.7\%$ per proton) was applied. The latter correction[9] used the proton asymmetry results from the CERN experiment.[3] No other corrections were made for the fact that the polarized neutron is embedded in the ^{3}He nucleus.

Scattered electrons with energy from 6 to 20 GeV were detected in two magnetic spectrometers centered at 4.5° and 7° respectively, as shown in Fig. 8. Each spectrometer was based on two large aperture dipole magnets bending in opposite directions. This 'reverse' deflection design[14] doubled the solid angle, integrated over the 6–20 GeV/c range, of the conventional design of same direction bending, used in previous polarized electron scattering experiments at SLAC.[2] The solid angle of the 4.5° arm was 0.15 msr and of the 7° arm was 0.5 msr. Each spectrometer was equipped with a pair of Čerenkov detectors, a pair of scintillator hodoscopes, and a lead-glass shower calorimeter.

Electrons were identified by a coincidence of the two Čerenkov counters and the shower counter. Hodoscope tracking was used for the absolute energy calibration of the shower counter and for studying backgrounds. The Čerenkov counters had

an efficiency of over 99% ($\sim$ 7 photoelectrons per incident electron). A typical Čerenkov counter pulse-height spectrum is shown in Fig. 9. The shower counters were ~98% efficient with a resolution (rms) of $15\%/\sqrt{E'}$.

The true asymmetries $A_\parallel$ and $A_\perp$ were derived from the measured raw asymmetries $(A_\parallel)_{\rm raw}$ and $(A_\perp)_{\rm raw}$:

$$A_\parallel = (A_\parallel)_{\rm raw} P_e P_t f \quad \text{and} \quad A_\perp = (A_\perp)_{\rm raw} P_e P_t f, \tag{12}$$

where P_e and P_t are the beam and target polarizations, respectively, and f is the fraction of events originating from polarized neutrons in the target. False asymmetries were found to be consistent with zero by comparing data with target spins in opposite directions (see Fig. 10).

The physics asymmetry A_1^n was extracted from the measured $A_\parallel$ and $A_\perp$ asymmetries:

$$A_1^n = \frac{A_\parallel}{(1+\eta\zeta)D} - \frac{\eta A_\perp}{(1+\eta\zeta)d} \tag{13}$$

and is shown for the three different beam energies of the experiment in Fig. 11. Here $\eta = \epsilon\sqrt{Q^2}/(E-\epsilon E')$, $\zeta = \eta(1+\epsilon)/(2\epsilon)$, and $d = D\sqrt{2\epsilon/(1+\epsilon)}$. Since no significant energy dependency of the measurement was observed, the A_1^n data were averaged and are shown in Fig. 12. Also shown in Fig. 12 are the data from the CERN SMC experiment.[15] The two data sets are consistent, showing a clear trend of negative asymmetries at low x.

The neutron spin function g_1^n was also calculated from the $A_\parallel$ and $A_\perp$ asymmetries,

$$g_1^n = \frac{MW_1^n}{(1+\gamma^2)(1+\eta\zeta)}\left[\frac{(1+\zeta\gamma)A_\parallel}{D} + \frac{(\gamma-\eta)A_\perp}{d}\right], \tag{14}$$

using values for the unpolarized W_1^n structure function and for R from a global fit of SLAC deep inelastic data.[16] Here $\gamma = \sqrt{Q^2}/\nu$. The neutron spin-structure function g_1^n is presented in Fig. 13.

The integral of the spin structure function over the measured x range 0.03 to 0.6 is $\int_{0.03}^{0.6} g_1^n(x)dx = -0.019 \pm 0.007$ (stat.) ± 0.006 (syst.) at an average Q^2 of 2 (GeV/c)^2. Evaluation of the integral at a constant Q^2 of 2 (GeV/c)^2, under the assumption that $A_1^n(x)$ is independent of Q^2, gives the same result. A correction for the unmeasured x range leads to the final result

$$\int_0^1 g_1^n(x)dx = -0.022 \pm 0.011. \tag{15}$$

The correction for $x < 0.03$ is based on an extrapolation that assumes a Regge parametrization[17] ($A_1^n \sim x^{1.2}$) and amounts to -0.006 ± 0.006. The correction for $x > 0.6$ assumes, as suggested by perturbative QCD in conjunction with quark-parton models, that $A_1^n \to 1$ for $x \to 1$. The high x extrapolation amounts to 0.003 ± 0.003. The final result is in agreement with the updated value[18] of the Ellis-Jaffe sum rule $\int_0^1 g_1^n(x)dx = -0.021 \pm 0.018$ at a Q^2 of 2 (GeV/c)^2.

The $\int_0^1 g_1^n(x)dx$ measurement can be used in the quark-parton model to extract the integrals Δq_i of the three quark spin distributions. Using the updated values for the hyperon decay constants $F = 0.47 \pm 0.04$ and $D = 0.81 \pm 0.03$ from Ref. 18, the measurement yields $\Delta u = 0.93 \pm 0.06$, $\Delta d = -0.35 \pm 0.04$, and $\Delta s = -0.01 \pm 0.06$. The sum $\Delta q = \Delta u + \Delta d + \Delta s$ of the three distributions is 0.57 ± 0.11, implying that the quarks account for approximately half of the nucleon spin. The remaining half could be attributed to contributions from orbital angular momentum[19,20] and the spin of the gluons.[21] A second implication is that the contribution from the strange sea is consistent with zero.

The new measurement on the neutron spin structure function integral can be combined with the previous measurement of the proton spin structure function integral to test the Bjorken sum rule. The result is

$$\int_0^1 \left[g_1^p(x) - g_1^n(x)\right]dx = 0.146 \pm 0.021 \tag{16}$$

for a Q^2 of 2 (GeV/c)^2. The Bjorken sum rule prediction using $\alpha_s = 0.39 \pm 0.10$ at $Q^2 = 2$ (GeV/c)^2 gives

$$\int_0^1 \left[g_1^p(x) - g_1^n(x) \right] dx = 0.183 \pm 0.007, \qquad (17)$$

which differs by about two standard deviations from the experimental value.

Part of the difference between the predicted and measured values can be attributed to higher-order perturbative QCD corrections to the Bjorken sum rule. The corrections[22] can be significant for the low Q^2 range of this experiment and can account for approximately half of the difference. Another possible correction[23] can arise from not theoretically well understood contributions from higher twist or target mass effects. Details on the interpretation of the experimental data can be found in recent theoretical investigations and reviews.[24-27]

In summary, new results on the neutron spin structure function have been presented. Within present theoretical uncertainties the results are consistent with the Bjorken sum rule prediction. They are in agreement with an updated value of the Ellis-Jaffe sum rule and suggest that the quarks account for about half of the nucleon spin. More precise data at higher Q^2 and lower x values will be beneficial for a better test of the Bjorken sum rule and for a clear interpretation of the spin structure functions in the context of the quark-parton model of the nucleon.

REFERENCES

1. M. J. Alguard *et al.*, Phys. Rev. Lett. **37**, 1258 (1976); **37**, 1261 (1976).
2. G. Baum *et al.*, Phys. Rev. Lett. **51**, 1135 (1983).
3. J. Ashman *et al.*, Nucl. Phys. **B238**, 1 (1989).
4. C. E. Carlson and W.-K. Tung, Phys. Rev. **D5**, 721 (1972).
5. A. J. G. Hey and J. E. Mandula, Phys. Rev. **D5**, 2610 (1972).
6. J. D. Bjorken, Phys. Rev. **148**, 1467 (1966); Phys. Rev. **D1**, 1376 (1970).
7. J. Kodaira *et. al.*, Phys. Rev. **D20**, 627 (1979); Nucl. Phys. **B159**, 99 (1979).
8. J. Ellis and R. Jaffe, Phys. Rev. **D9**, 1444 (1974).
9. C. Ciofi degli Atti *et al.*, Phys. Rev. **C48**, 968 (1993).
10. R. Shulze and P. Sauer, Phys. Rev. **C48**, 38 (1993).
11. R. M. Woloshyn, Nucl. Phys. **A496**, 749 (1989).
12. T. E. Chupp *et al.*, Phys. Rev. **C36**, 2244 (1987); **C45**, 915 (1992).
13. H. Middleton *et al.*, in Proceedings of Workshop on Polarized Gas Targets, Madison, WI, May 1993.
14. G. G. Petratos *et al.*, SLAC-PUB-5678 (1991).
15. B. Adeva *et.al.*, Phys. Lett. **B362**, 553 (1993).
16. L. W. Whitlow *et al.*, Phys. Lett. **B250**, 193 (1990); **B282**, 475 (1992).
17. A. Schafer, Phys. Lett. **B208**, 175 (1988).
18. R. L. Jaffe and A. V. Manohar, Nucl. Phys. **B337**, 509 (1990).
19. L.M. Sehgal, Phys. Rev. **D10**, 1663 (1974).
20. J. Ellis and M. Karliner, Phys. Lett. **B213**, 73 (1988).
21. G. Altarelli and G. G. Ross, Phys. Lett. **B212**, 391 (1988)

22. S. A. Larin and J. A. M. Vermaseren, Phys. Lett. **B259**, 345 (1991).

23. I. I. Balitsky *et al.*, Phys. Lett. **B242**, 245 (1990).

24. F. E. Close, Rutherford prepring RAL-93-040 (1993).

25. G. Preparata and P. Ratcliffe, Milano preprint MITH-93/15 (1993).

26. J. Ellis and M. Karliner, CERN preprint CERN-TH-7022/93 (1993).

27. X. Ji and P. Unrau, MIT preprint MIT-CTP-2232 (1993).

FIGURE CAPTIONS

1. The polarized electron source set-up.
2. A typical Møller elastic peak (top) and its asymmetry (bottom).
3. The incident beam polarization measured in the Møller spectrometer. The data runs span a two-month period.
4. A theoretical calculation[9] for the ^{3}He and neutron spin structure function. Solid curve: g_1 of ^{3}He; short-dashed curve: neutron contribution; long-dashed curve: proton contribution; dotted curve: g_1 for a free neutron.
5. The polarized ^{3}He target set-up.
6. a) Typical signal of the ^{3}He cell NMR measurement; b) Typical signal of the water cell MNR measurement.
7. The ^{3}He target cell polarization from the NMR measurements. The data runs span a two-month period.
8. The two magnetic spectrometers and detectors.
9. Typical pulse-height spectrum for one of the Čerenkov counters.
10. Cross-section asymmetry for target spins in opposite direction indicating that a false asymmetry is consistent with zero (x^2 per degree of freedom = 1.1).
11. The neutron A_1^n asymmetry for the three beam energies of the experiment.
12. The neutron A_1^n asymmetry averaged over beam energies. Also shown are the A_1^n data from the CERN SMC experiment.
13. The g_1^n spin structure function of the neutron.

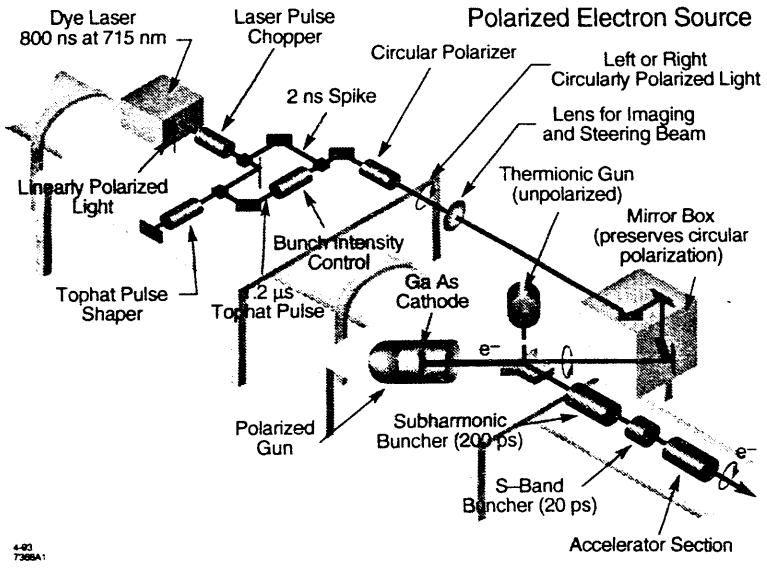
Polarized Electron Source
Dye Laser
800 ns at 715 nm
Laser Pulse
Chopper
Circular Polarizer
Left or Right
Circularly Polarized Light
2 ns Spike
Lens for Imaging
and Steering Beam
Linearly Polarized
Light
Thermionic Gun
(unpolarized)
Mirror Box
(preserves circular
polarization)
Bunch Intensity
Control
Tophat Pulse
Shaper
.2 μs
Tophat Pulse
Ga As
Cathode
e⁻
Polarized
Gun
Subharmonic
Buncher (200 ps)
e⁻
S-Band
Buncher (20 ps)
Accelerator Section
4-93
7368A1

Fig. 1

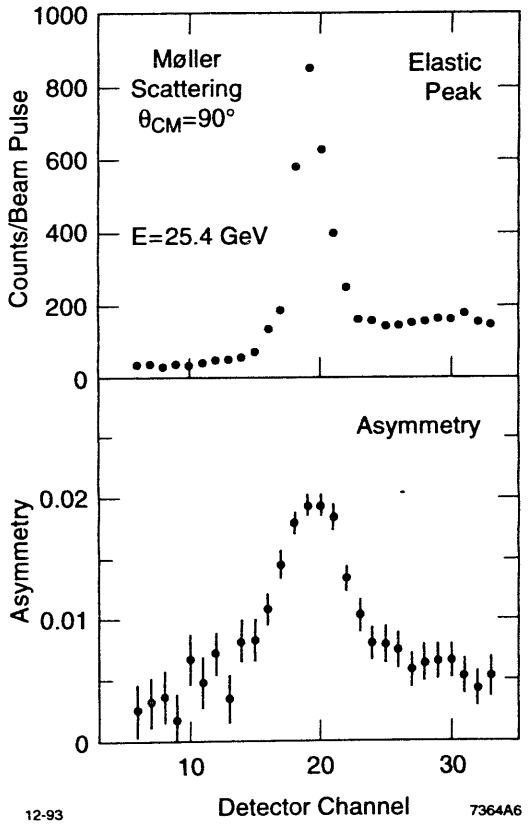
Counts/Beam Pulse
1000
800
600
400
200
0
Møller
Scattering
θCM=90°
Elastic
Peak
E=25.4 GeV
Asymmetry
Asymmetry
0.02
0.01
0
10
20
30
Detector Channel
12-93
7364A6

Fig. 2

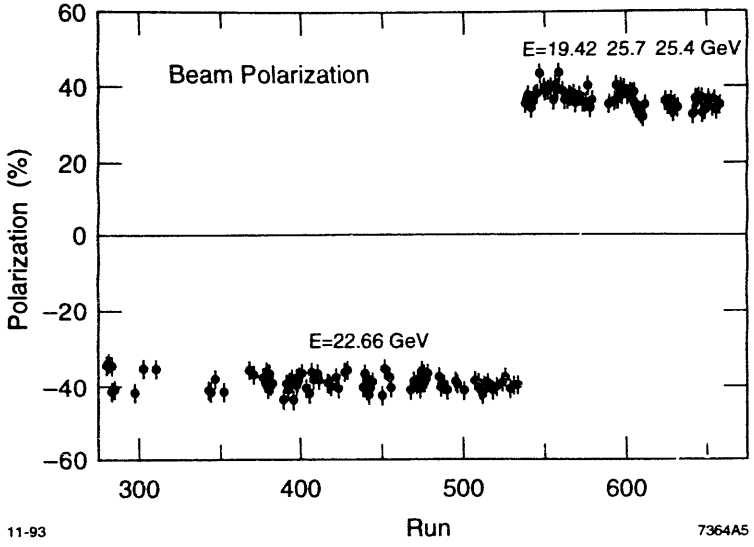
Beam Polarization
E=19.42 25.7 25.4 GeV
E=22.66 GeV
Polarization (%)
60
40
20
0
−20
−40
−60
300
400
500
600
Run
11-93
7364A5

Fig. 3

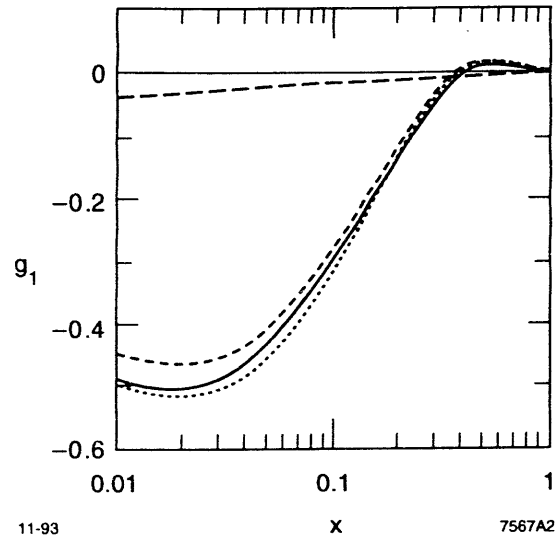
g_1
0
−0.2
−0.4
−0.6
0.01
0.1
1
x
11-93
7567A2

Fig. 4

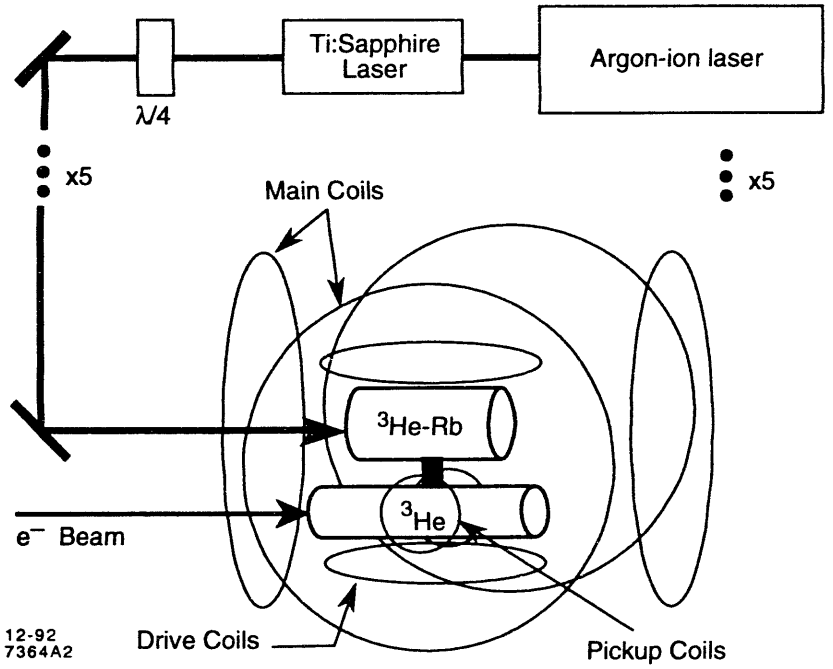
Ti:Sapphire Laser
Argon-ion laser
λ/4
x5
x5
Main Coils
^{3}He-Rb
^{3}He
e$^-$ Beam
12-92
7364A2
Drive Coils
Pickup Coils

Fig. 5

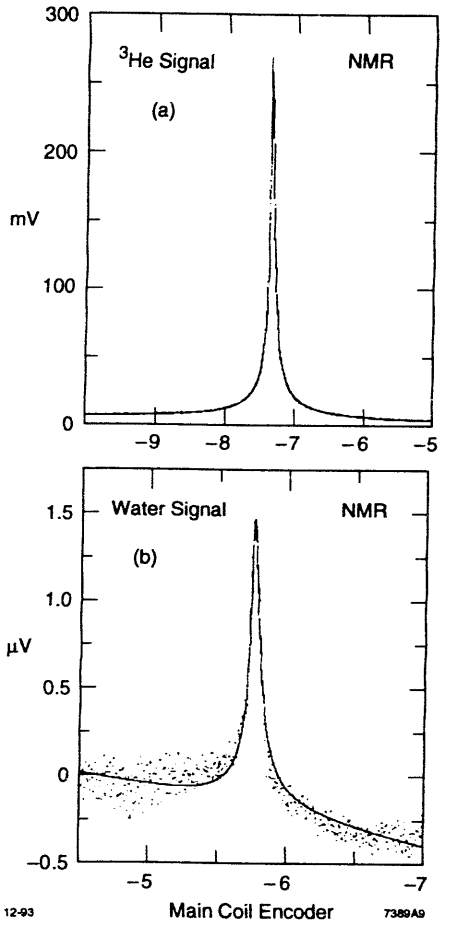
^{3}He Signal
NMR
(a)
mV
300
200
100
0
−9
−8
−7
−6
−5
Water Signal
NMR
(b)
μV
1.5
1.0
0.5
0
−0.5
−5
−6
−7
12-93
Main Coil Encoder
7389A9

Fig. 6

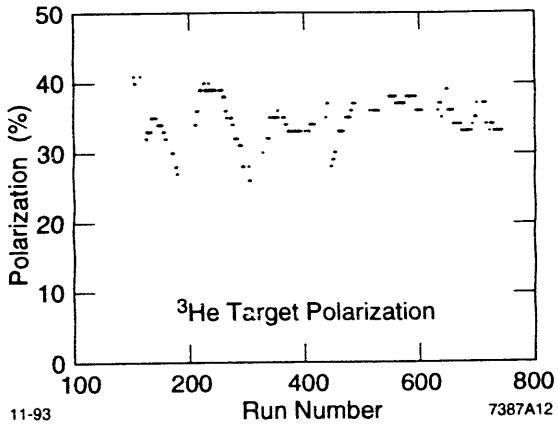
50
40
30
20
10
0
Polarization (%)
^{3}He Target Polarization
100
200
400
600
800
Run Number
11-93
7387A12

Fig. 7

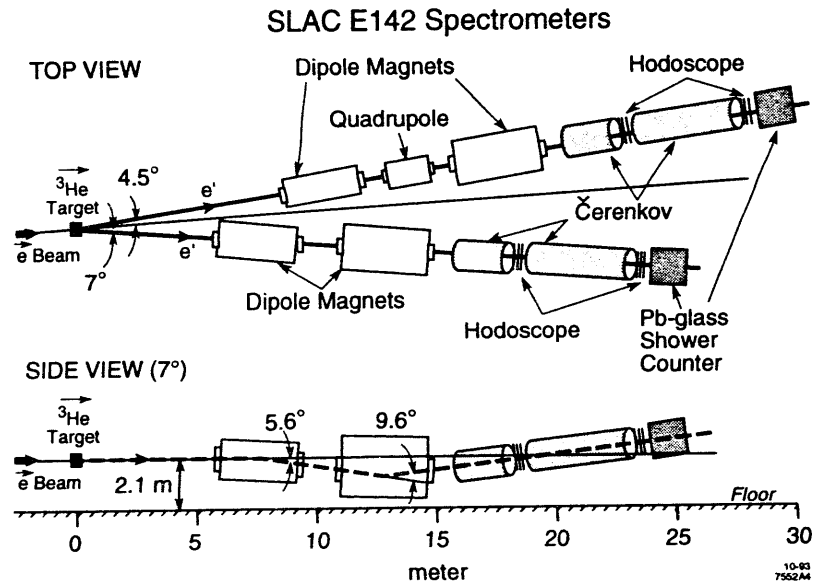
SLAC E142 Spectrometers
TOP VIEW
Dipole Magnets
Hodoscope
Quadrupole
^{3}He Target
4.5°
e'
Čerenkov
e Beam
e'
7°
Dipole Magnets
Hodoscope
Pb-glass Shower Counter
SIDE VIEW (7°)
^{3}He Target
5.6°
9.6°
e Beam
2.1 m
Floor
0
5
10
15
20
25
30
meter
10-93
7552A4

Fig. 8

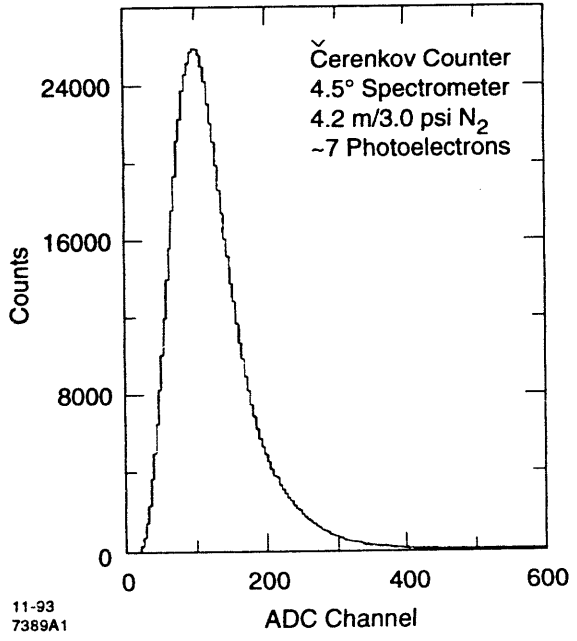
Čerenkov Counter
4.5° Spectrometer
4.2 m/3.0 psi N_2
~7 Photoelectrons
Counts
24000
16000
8000
0
0
200
400
600
ADC Channel
11-93
7389A1

Fig. 9

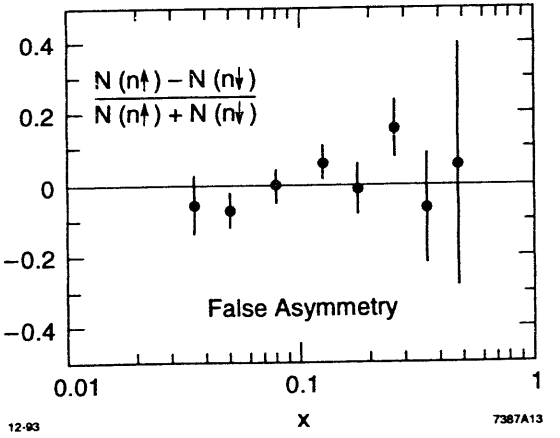
0.4
0.2
0
−0.2
−0.4
$\frac{N(n\uparrow) - N(n\downarrow)}{N(n\uparrow) + N(n\downarrow)}$
False Asymmetry
0.01
0.1
1
x
12-93
7387A13

Fig. 10

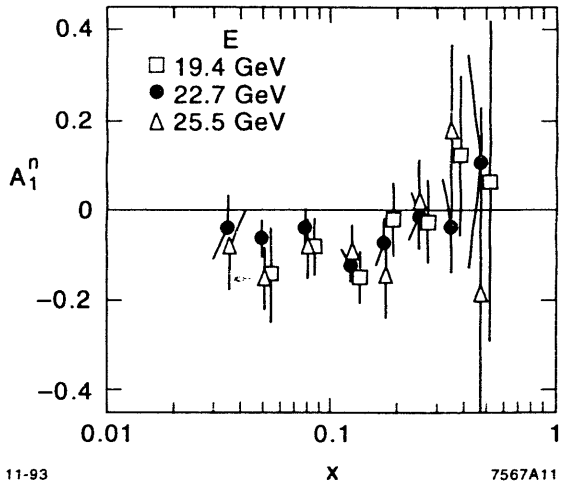
E
□ 19.4 GeV
● 22.7 GeV
△ 25.5 GeV
A_1^n
0.4
0.2
0
−0.2
−0.4
0.01
0.1
1
x
11-93
7567A11

Fig. 11

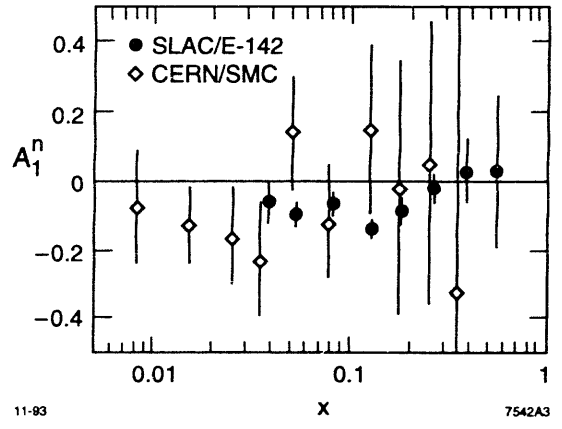
● SLAC/E-142
◇ CERN/SMC
A_1^n
0.4
0.2
0
−0.2
−0.4
0.01
0.1
1
x
11-93
7542A3

Fig. 12

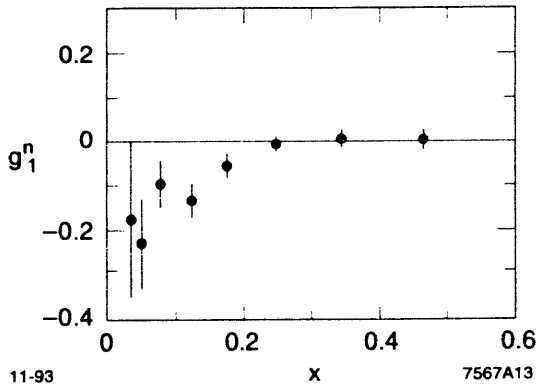

Fig. 13

END

DATE
FILMED
3/4/94